# KATANIN-dependent mechanical properties of the stigmatic cell wall regulate pollen tube pathfinding

Lucie Riglet[1], Frédérique Rozier[1], Chie Kodera[1], Isabelle Fobis-Loisy[1*] and Thierry Gaude[1*]

[1]Laboratoire de Reproduction et Développement des Plantes, Université de Lyon, ENS de Lyon, UCBL, INRA, CNRS, 46 Allée d'Italie, 69364 Lyon Cedex 07, France

*e-mail: thierry.gaude@ens-lyon.fr ; isabelle.fobis-loisy@ens-lyon.fr

## ABSTRACT

Successful fertilization in angiosperms depends on the proper trajectory of pollen tubes through the pistil tissues to reach the ovules. Pollen tubes start their path by progressing within the cell wall of the papilla cells, applying pressure to the wall. Mechanical forces are known to play a major role in plant cell shape by controlling the orientation of cortical microtubules (CMTs), and hence deposition of cellulose microfibrils (CMFs). Here, by combining cell imaging and genetic approaches, we show that isotropic orientation of CMTs in aged, *katanin1-5* (*ktn1-5*) or oryzalin-treated papilla cells is accompanied by a tendency of pollen tubes to coil around the papillae. In addition, using atomic force microscopy, we uncover that aged and *ktn1-5* papilla cells have a softer cell wall. Altogether, our results suggest that KATANIN-dependent control of microtubule dynamics, and associated mechanical anisotropy of stigmatic walls, mediate pollen tube growth directionality.

## INTRODUCTION

Following deposition of dehydrated pollen grains on the receptive surface of the female organ, the stigma, pollen rehydrates, germinates and produces a pollen tube that carries the male gametes toward the ovules where the double fertilization takes place. This long itinerary through the different tissues of the pistil is finely controlled, avoiding misrouting of the pollen tube and hence assuring proper delivery of the sperm cells to the female gametes. In *Arabidopsis thaliana*, pollen tubes grow within the cell wall of papillae of the stigmatic epidermis, and then through the transmitting tissue of the style and ovary[1]. The transmitting tissue has an essential function in pollen tube guidance, providing chemical attractants and nutrients[2,3]. In contrast to these accumulating data showing the existence of factors mediating pollen tube growth in the pistil, whether guidance cues exist at the very early stage of pollen tube emergence and growth in the papilla cell wall remains largely unknown. The cell wall constitutes a stiff substrate and hence a mechanical barrier to pollen tube progression. There are numerous examples in animal cells demonstrating that mechanical properties of the cellular environment, and in particular rigidity, mediate cell signalling,

proliferation, differentiation and migration[4–6]. In plant cells, cell wall rigidity depends mainly on its major component, cellulose, which is synthesized by plasma membrane-localized cellulose synthase complexes (CSCs) moving along cortical microtubule (CMT) tracks[7]. While penetrating the cell wall, the pollen tube exerts a pressure onto the stigmatic cell[8]. Such physical forces are known to reorganize the cortical microtubules (CMTs), which by directing CSCs to the plasma membrane, reinforce wall stiffness by novel cellulose microfibril (CMF) synthesis[9,10]. Hence, there is an intricate interconnection between CMT organization, CMF deposition and cell wall rigidity[11,12]. A major regulatory element of CMT dynamics is the KATANIN (KTN1) microtubule-severing enzyme, which allows CMT reorientation following mechanical stimulation[10,13,14]. Here we investigated whether the CMT network of papilla cells might contribute to pollen tube growth and guidance in stigmatic cells by combining cell imaging and genetic approaches. We found that CMT network of papilla cells is modified with ageing, CMT bundles being anisotropic at anthesis and becoming isotropic at later stages of stigma development. This change in CMT organization was accompanied by a modification of the direction of pollen tube growth, which passes from predominantly straight to coiled. In the *ktn1-5* mutant, papilla cells exhibited a strong CMT isotropy associated with a marked tendency of wild-type (WT) pollen tubes to turn around the papilla. Coiled growth of pollen tubes was also observed on stigma papillae treated with the CMT-depolymerizing drug oryzalin, although at a lower extent. Faster growth of coiled pollen tubes was observed in aged WT as well as *ktn1-5* papillae, which both were found to exhibit softer cell walls. Additionally, we tested a series of cell wall mutants, including mutants having CMT disorganization and decreased cell wall rigidity and, unexpectedly, none of them used as female induced coiled growth of WT pollen tubes. Altogether, our results strongly suggest that CMT organization and cell wall mechanical properties dependent on KTN1 have a major role in guiding early pollen tube growth in stigma papillae.

## RESULTS

**CMT dynamic pattern and pollen tube growth during stigma development.** To assess the functional role of stigmatic CMTs in pollen – papilla cell interaction, we first analysed their organization in papillae at stages 12 to 15 of stigma development as described[15] (Fig. 1a,b). We generated a transgenic line expressing the CMT marker MAP65.1-citrine under the control of the stigma specific promoter SLR1[16]. Before (stage 12) and at anthesis (stage 13), the CMTs were aligned perpendicularly to the longitudinal axis of papilla cells and were highly anisotropic (median value of 0.40) (Fig. 1c,d). At stage 14, when anthers extend above the stigma, the CMT pattern became less organized, with a higher variability in anisotropy values. Finally, at stage 15 when the stigma extends above anthers, CMT anisotropy had a

median value of 0.09 indicative of an isotropic orientation of CMTs (Fig. 1c,d). These findings reveal that the papilla CMT cytoskeleton is dynamic during development, with a change of CMT array orientation from anisotropy to isotropy. We then wondered whether this change in CMT organization could be correlated with pollen tube growth. To this end, we self-pollinated Col-0 papillae from stages 12 to 15 and examined pollen tube growth one hour after pollination by scanning electron microscopy (SEM) (Fig. 2a). At stage 12 and 13, we found most (~60%) pollen tubes to grow straight in the papillae, whereas about 30% and 10% of tubes made half-turn or one turn around stigmatic cells, respectively (Fig. 2b). At later stages of development, the tendency to coil around the papillae dramatically increased, with more than 35% of pollen tubes at stage 14 and more than 55% at stage 15 making one or more than one turn around papillae. These results suggest that CMT organization in the papilla impacts the direction of growth of pollen tubes and that loss of CMT anisotropy is associated with coiled growth.

**Impaired CMT dynamics of papillae affects pollen tube growth direction.** To confirm the relation between stigma CMTs and pollen behaviour, we examined pollen tube growth on stigmas of the *katanin1-5* mutant, which is known to exhibit reduced CMT array anisotropy in root cells[17–19]. Because the CMT organization in *ktn1-5* papillae is unknown, we crossed *ktn1-5* with the MAP65-1-citrine marker line and found that CMT arrays were more isotropic in *ktn1-5* papillae when compared with those of the WT (Fig. 3a,c). Using SEM, we then analysed Col-0 pollen behaviour on *ktn1-5* stigmatic cells at stage 13 (Fig. 3b). We observed that Col-0 pollen tubes acquired a strong tendency to coil around *ktn1-5* papillae, with above 60% of tubes making one or more than one turn around papillae, sometimes making up to 6 turns, before reaching the base of the cell (Fig. 3d and Supplementary Fig. 1a). In some rare cases, pollen tubes even grew upward in the *ktn1-5* mutant and appeared blocked at the tip of the papilla (Supplementary Fig.1b). To test the direct impact of stigma CMTs on pollen tube growth direction, we examined whether the destabilization of CMTs in Col-0 papillae could affect pollen tube growth. To this end, we treated stigmas by local application of the depolymerizing microtubule drug oryzalin in lanolin pasted around the style. After 4 hours of drug treatment, no more CMT labelling was detected in papillae, while CMTs were clearly visible in mock-treated (DMSO) stigmas (Fig. 4a). Stigmas were then pollinated with Col-0 pollen and one hour later, pollen tubes were found turning on drug-treated but not on control papillae (Fig. 4b,c). However, the number of coils was significantly lower than on *ktn1-5* papillae. Indeed, 25% of the pollen tubes made at least 2 coils in *ktn1-5* papillae whereas this percentage represented only 4% on the oryzalin treated stigmas (Fig. 3d,4c). Altogether, these results confirm that stigmatic CMTs contribute to the directional growth of pollen tubes in papilla cells.

**Mechanical properties of the cell wall are disturbed in *ktn1-5* papilla cells.** Because the main role of CMTs in plant cells is to guide the trajectory of CSCs, thereby impacting the mechanical anisotropy of the cell wall, we analysed the cell walls of Col-0 and *ktn1-5* papillae following pollination. First, using Transmission Electron Microscopy (TEM), we found Col-0 pollen tubes to penetrate the cuticle and to grow between the two layers of the papilla cell wall, as previously described[20], in both Col-0 and *ktn1-5* papilla cells (Fig. 5a). We did not detect any significant difference in the ultrastructure of cell walls (Supplementary Fig. 2). Interestingly, as the pollen tube progresses through the papilla cell wall, it generates a bump (external deformation) and an invagination (internal deformation) in the cell wall. As such deformations could reflect differences in wall properties, we quantified the external (extD) and internal (intD) deformation following pollination of Col-0 and *ktn1-5* stigmas. To visualize more clearly this deformation, we pollinated stigmas expressing the plasma membrane protein LTI6B fused to GFP (LTI6B-GFP) with pollen whose tube was labelled with the red fluorescent protein RFP driven by the ACT11 promoter[21] (Fig. 5b). We found that Col-0 pollen tubes grew with almost equal extD and intD values in Col-0 cell wall. However, the ratio between extD and intD was about 3 when Col-0 pollen tubes grew in *ktn1-5* papilla cells (Fig. 5b,c,d). These quantitative data are consistent with the observation of major protuberances caused by pollen tubes on *ktn1-5* stigmatic cells using SEM (Fig. 3b and Supplementary Fig. 1). Assuming that stigmatic cells are pressurized by their turgor pressure, this may reflect the presence of softer walls in *ktn1-5* papillae. To test this hypothesis, we assessed the stiffness of Col-0 and *ktn1-5* papilla cell walls using Atomic Force Microscopy (AFM) with a 400 nm indentation. We found that cell wall stiffness in *ktn1-5* papilla cells was about 30% lower than that in stage 13 WT cells (Fig. 5e,f). To confirm this result, we investigated the stiffness of the papilla cell wall on WT stigmas at stage 15, where increased coiled pollen tubes were detected (Fig. 2 a,b). We found the cell wall to be softer than that of papillae at stage 13 but stiffer than that of the *ktn1-5* (Fig. 5e,f). We then reasoned that the presence of softer walls should also affect the pollen tube growth rate, stiffer walls reducing growth. We thus monitored the growth rate of Col-0 pollen tubes in Col-0 and *ktn1-5* papillae. We found that pollen tubes grew faster (~ x 1.8) within *ktn1-5* papillae (Fig. 5g). Similarly, we found that pollen tube growth on stage 15 papillae was faster (~ x 1.6) than on stage 13 papillae (Fig. 5h). Altogether, these results suggest that KATANIN-dependent mechanical properties of papilla cell wall impact pollen tube growth.

**Defects in papilla cell-wall composition are not sufficient to affect Col-0 pollen tube behaviour.** The *katanin1/fra2* mutant was initially described as a mutant impaired in cell wall biosynthesis and CMT array organization[19]. This prompted us to test whether other mutants affected in cell wall biogenesis might exhibit the coiled pollen tube phenotype. Indeed, in the

simplest scenario, the presence of softer walls, whatever the cause, may be sufficient to induce extra coiling due to faster pollen tube growth. We selected mutants impaired in the cellulose synthase complex (*kor1.1*, *prc1* and *any1*), hemicellulose biosynthesis (*xxt1 xxt2*, *xyl1.4*) and pectin content (*qua2.1*) (Supplementary Table 1). Strikingly, none of the 6 cell wall mutants displayed the coiled pollen tube phenotype (Supplementary Fig. 3). This suggests that the relation between CMT organisation, cell wall stiffness and pollen tube trajectory is stricter than anticipated. Because CMTs guide cellulose deposition, they also control the directional elongation of plant cells[22]. The contribution of stigmatic CMTs to pollen tube growth may thus be mediated by papilla cell shape only. For instance, wider cells in *ktn1-5* would promote pollen tube coiling. To check that possibility, we measured the length and width of papilla cells in Col-0 (at stage 13 and 15), *ktn1-5, xxt1 xxt2* and *any1* (Supplementary Fig. 4). We did not find any correlation between papilla length and the coiled phenotype. Indeed, coiled phenotype was observed in stage-15 WT papillae that were longer than those at stage-13, as well as in *ktn1-5* papillae that had a length similar to stage-13 WT papillae. The correlation between papilla width and coiled phenotype was also not clear-cut. As expected, *ktn1-5* mutant exhibited wider papillae than Col-0. Stage-15 WT papillae were also significantly larger than stage-13 WT papillae, where coils were observed. However, *xxt1 xxt2* and *any1* papillae were also wider than the WT but did not display the coiled phenotype. Altogether, this suggests that papilla morphology is not sufficient to explain the coiled phenotype. Because CMT disorganization in papillae affects both wall stiffness and mechanical anisotropy, we next investigated the relative contribution of these two parameters in pollen tube growth. We focused our analysis on the *xxt1 xxt2* double mutant. Indeed, this mutant was reported to display CMT orientation defects and a softer cell wall in hypocotyl cells, when compared with the WT[12]. As the pollen tube phenotype on *xxt1 xxt2* stigmas was similar to the WT, we wondered whether the cell wall stiffness of stigmatic cells was actually affected in these mutant papillae. Using AFM, we found the papilla cell wall of the mutant to be about 30% softer than that of Col-0 papillae, i.e. very similar to that of *ktn1-5* (Fig. 5f). However, despite this similarity, the pollen tube growth rate in *xxt1 xxt2* stigmas was identical to Col-0 stigmas at stage 13 (Fig. 5h). In addition, contrary to *ktn1-5*, we did not observe external bumps on *xxt1 xxt2* papillae when pollen tubes were growing (Supplementary Fig. 3g). These results indicate that alteration of the cell wall stiffness alone is not sufficient to induce the pollen tube coiled phenotype and promote tube growth speed, and suggest that, instead, the mechanical anisotropy of cell walls plays a key role in pollen tube trajectory.

## DISCUSSION

How the pollen germinates a tube and how pollen tube growth is regulated have been the object of many investigations[23,24]. The use of in vitro pollen germination as well as semi-in vivo fertilization assays, together with the analysis of mutants defective in pollen or ovule functions, have rapidly expanded our knowledge of the mechanisms that sustain pollen tube growth, its guidance toward the ovule and the final delivery of male gametes within the embryo sac[25–27]. At the cellular level, cytoskeleton has been extensively studied during pollen tube elongation[28], highlighting the critical role played by the actin microfilaments in pollen-tube tip growth through delivery of materials for the biosynthesis of the plasma membrane and cell wall. By contrast, CMTs seem to have a lower importance in this process, drugs affecting CMT polymerisation having no significant effects on pollen-tube growth rate, yet altering the capacity of pollen tubes to change their growth direction[29]. Rearrangements of actin microfilaments[30] and destabilization of CMTs[31] have been described in stigmas following compatible pollination in Brassica species. However, CMT pattern and dynamics during papilla development have never been reported. Our data show that during the course of stigma maturation, which is associated with papilla cell elongation (Supplementary Fig. 4a,b), CMT bundles progressively move from perpendicular (anisotropic) to the elongation axis at stage 12 to disorganised (isotropic) at stage 15. This correlates with the known CMT dynamics during elongation in plant cells, where CMT arrays are highly anisotropic in young cells and become more isotropic as cells differentiate[22,32]. The progressive randomisation of CMT orientation in papilla cells is accompanied by an increased coiled growth of pollen tubes in papillae. Similarly, when CMTs are destabilized by the microtubule depolymerizing drug oryzalin, coiled pollen tubes are more frequently observed compared with untreated control stigmas. These results reveal a link between the stigmatic CMT cytoskeleton organization and the trajectory that pollen tube takes while growing in the papilla cell wall. The fact that the most striking effect on pollen tube growth was found on *ktn1-5* mutant suggests that the coiled phenotype depends not only on the CMT organization but implicates other factors. Among various phenotypic alterations described in loss-of-function mutants for *KTN1*, are the impaired cell mechanical properties and cell elongation, defects in CMT organization, cell wall composition and CMF orientation[18,19,33]. Interestingly, we found that the protuberance of pollen tubes at the surface of *ktn1-5* papillae was associated with a faster growth rate and a lower rigidity of the cell wall compared with Col-0. This places mechanics of the cell wall as a likely component involved in the coiled phenotype. Surprisingly, cell wall mutants, such as *xxt1 xxt2* and *prc1*, known to exhibit both abnormal CMT organization and softer cell walls, and somehow that may share mechanical properties with *ktn1-5*, did not induce the coiled phenotype displayed by *ktn1-5* papillae. More remarkably, despite the similar stiffness of *xxt1*

*xxt2* and *ktn1-5* papilla cell walls measured in our AFM experiments, pollen tubes behaved differently on these two stigmas. This indicates that components other than cell wall stiffness are involved in the pollen tube coiled phenotype and that mechanical properties of the cell wall are likely not identical in the two mutants. Indeed, though sharing a similar alteration of cell wall stiffness, the global plant morphology of these mutants is clearly distinct. The *ktn1-5* mutant was described to have a severe reduction in cell length and an increase in cell width in all organs[19]. This cellular phenotype was attributed to the distorted deposition of CMFs correlated with the isotropic orientation of CMTs, whereas in WT cells CMFs, like CMTs, are oriented perpendicularly to the elongation axis[18]. We also found larger papilla cells for *ktn1-5* (Supplementary Fig. 4c,d), supporting the hypothesis that orientation of CMFs is also altered in *ktn1-5* papillae. Hence, we may assume that mechanical anisotropy, described as the cell wall anisotropy made by the orientation of the rigid CMFs[34], is impaired in *ktn1-5* papillae. By contrast, the *xxt1 xxt2* double mutant, although deprived of xyloglucans in its cell walls, shows a growth phenotype[35,36] not as severe as *ktn1-5*. In etiolated hypocotyls, contrary to Col-0, CMFs are largely parallel to one another, straighter than in WT and oriented approximately transversely to the long axis of the cell[12]. Interestingly, we found the papilla cell shape of *xxt1 xxt2* stigmas to be similar to Col-0, though with slightly wider papillae (Supplementary Fig. 3g,4e,f). However, *xxt1 xxt2* papillae were less wide than *ktn1-5* papillae, which is consistent with an anisotropic growth of the papillae in the *xxt1 xxt2* mutant compared with *ktn1-5*. At the cell wall level, apart from a similar stiffness, the main differences between *ktn1-5* and *xxt1 xxt2* appear to be the cell wall composition, orientation of CMFs and possible changes in molecular connections between cell wall components and plasma membrane and/or cytoskeleton proteins. Indeed, a recent proteomic study revealed that loss of KATANIN function is associated with the decrease in abundance of several cytoskeleton proteins, such as profilin 1, actin-depolymerizing factor 3 and actin 7[37], whereas targeted quantitative RT-PCR unveiled that Microtubule-associated protein (MAP) and wall signal receptor genes are downregulated in *xxt1 xxt2*[12]. In this latter study, KTN1 expression level was shown to be unchanged compared with Col-0. Altogether, our study suggests that KTN1, by maintaining the papilla mechanical anisotropy, has a key function in mediating early pollen tube guidance on stigma papillae.

The coiled phenotype was not only observed in *ktn1-5* but also in the WT Col-0 papillae at stage 15. This is likely to be related to isotropic orientation of CMTs and CMFs known to occur during cell elongation[38,39]. At the organ level, it has been suggested that the mechanical anisotropy of the wall restrains organ emergence[34]. The authors propose that for the same wall stiffness, a cell wall with isotropic properties would lead to larger outgrowth than a wall with anisotropic properties. Our data are consistent with this hypothesis, albeit at

the subcellular scale, since large protuberance of papilla wall following pollen tube growth is observed in *ktn1-5* papilla cells, exhibiting walls with isotropic properties.

It remains unclear how mechanical anisotropy guides pollen tube growth. We can hypothesise that as pollen tube grows inside the wall, it encounters recently deposited CMFs on the inner side of the wall (facing the cytoplasm) and older CMFs on the outer side. It is likely that these layers have different mechanical properties related to CMF orientation[22]. Pollen tubes may grow helically by default, as is the case for climbing plants around a cylindrical substrate but the presence of a mechanically reinforced inner wall may slow down and bias the trajectory of the pollen tube. It is worth noting that growth rate is slowed down when pollen tubes pass through a microgap of a microfluiding device, the tubes adapting their invasive force to the mechanical constraints[40]. Our data show that the pollen tube tip, while progressing in the papilla wall, senses the mechanical features of its environment and reacts accordingly. Hence, it reveals some unanticipated internal and hidden properties of the cell wall. Interestingly, recent work showed that axons were capable of adapting their growth rate and direction according to mechanical constraints, growing straighter on rigid substrate underlining that mechanical signals are important regulators of pathfinding[41].

In the last decades, many studies pointed out that chemical but also mechanical components must be considered to be implicated in pollen tube growth direction[25]. Implication of chemical cues for pollen tube guidance in the stigma remains largely unknown, although the blue copper protein plantacyanin, when overexpressed in Arabidopsis stigmas, was reported to be a possible guidance factor through an as yet undiscovered mechanism [42]. However, no defect in pollen tube growth directionality was detected in a know-down plantacyanin mutant, questioning the actual role of this protein as a chemoattractant in Arabidopsis. In our study, we add mechanics as a key player in early pollen tube guidance in the papilla cell. Our results suggest that this role is mediated by a specific CMT organization and mechanical anisotropy of the papilla cell, which both are dependent on KTN1. Importantly, KTN1 prevents emerging pollen tubes to grow upward on papilla cells and straightens pollen tube direction, helping the tube to find its correct path to the stylar transmitting tract. This highlights an yet unexpected role for KTN1 in pollen tube guidance, which was until now mostly known to be involved in plant development and stress-response regulation. In addition, our study also clearly unveils the fact that the mechanical properties of one single cell (e.g., the stigmatic papilla) impact the behaviour of its neighbouring cell (e.g., the pollen tube).

## MATERIALS AND METHODS

**Plant Materials and Growth Conditions.** *Arabidopsis thaliana*, ecotype Columbia (Col-0), *Arabidopsis* transgenic plants generated in this study and *Arabidopsis* mutants were grown in soil under long-day conditions (16 hours of light / 8 hours of dark, 21°C / 19°C) with a relative humidity around 60%. *ktn1-5* (SAIL_343_D12), *xxt1xxt2*, *prc1.1, qua2.1*, *xyl1.4*, *kor1.1* and *any1* mutant lines were described previously[35,43–49]. All mutants were in Col-0 background except *kor1.1* which was in WS.

**Plasmid construction.** We used the Gateway® technology (Life Technologies, USA) and two sets of Gateway®-compatible binary T-DNA destination vectors[50,51] for expression of transgenes in *A. thaliana*. The DNA fragment containing the *Brassica oleracea SLR1* promoter was inserted into the pDONP4-P1R vector. The 165 bp-*LTI6B* fragment was introduced into the pDONR207 vector. *MAP65* gene spanning the coding region from start to stop codons was introduced into the pDONR221 vector. CDS from citrine or GFP were cloned into the pDONP2R-P3 vector. Final constructs, pSLR1::MAP65-citrine and pSLR1::LTI6B-GFP were obtained by a three-fragment recombination system (Life Technologies) using the pK7m34GW and the pB7m34GW destination vectors, respectively. We generated a pAct11::RFP construct by amplifying the promoter of the *A. thaliana Actin 11* gene and cloning it into the pGreenII gateway vector in front of the RFP coding sequence.

**Generation of transgenic lines and crossing**. Transgenic lines were generated by *Agrobacterium tumefaciens*-mediated transformation of *A. thaliana* Col-0 as described[52]. Unique insertion lines, homozygous for the transgene were selected. We introduced the pSLR1::LTI6B-GFP or pSLR1::MAP65-citrine construct in *ktn1-5* background by crossing and further selecting the progeny on antibiotic containing medium.

### Microscopy

***Confocal microscopy.*** Flowers at stages 12 to 15[15] collected from fluorescent lines were emasculated and stigmas were observed under a Zeiss LSM800 microscope (AxioObserver Z1) using a 40x Plan-Apochromat objective (numerical aperture 1.3, oil immersion). Citrine was excited at 515 nm and fluorescence detected between 530 and 560nm. GFP was excited at 488 nm and fluorescent detected between 500 and 550 nm. RFP was excited at 561 nm and fluorescent detected between 600 and 650 nm.

***Live imaging*.** Flowers from stages 12 to 15 were emasculated and pollinated on plants with mature pollen from the pACT11::RFP line. Immediately after pollination, stigmas were mounted between two coverslips. To maintain a constant humidity without adding liquid

directly on the stigma surface, we use a wet piece of tissue in contact with the base of the stigma. Pollinated stigmas were observed under a Zeiss microscope (AxioObserver Z1) equipped with a spinning disk module (CSU-W1-T3, Yokogawa) using a 40x Plan-Apochromat objective (numerical aperture 1.1, water immersion). Serial confocal images were acquired in the entire volume of the stigma every 1 µm and every minute. Images were processed with Image J software and pollen tube lengths were measured.

***Atomic Force Microscopy*.** Pistils at stage 13 were placed straight in a 2% agar MS medium and 0.8% low-melting agarose was added up to the base of papilla cells. AFM indentation experiments were carried out with a Catalyst Bioscope (Bruker Nano Surface, Santa Barbara, CA, USA) that was mounted on an optical microscope (MacroFluo, Leica, Germany) equipped with a x10 objective. All quantitative measurements were performed using standard pyramidal tips (RFESP-190 (Bruker)). The tip radius given by the manufacturer was 8-12 nm. The spring constant of the cantilever was measured using the thermal tune method and was 35 N/m. The deflection sensitivity of the cantilever was calibrated against a sapphire wafer. All experiments were made in ambient air at room temperature. Matrix of 10x10 measurements (step 500 nm) was obtained for each papilla, with a 1µN force. The Young's Modulus was estimated using the Nanoscope Analysis (Bruker) software, using the Sneddon model with a < 200nm indentation.

***Environmental Scanning Electron Microscopy (SEM)*.** Flowers from stages 12 to 15 were emasculated and pollinated on plants with mature WT pollen. One hour after pollination, pistils were cut in the middle of the ovary, deposited on a SEM platform and observed under Hirox SEM SH-3000 at -20°C, with an accelerating voltage of 15kV. Images were processed with ImageJ software and pollen tube direction was quantified by counting the number of turns made by the tube, only on papillae that received one unique pollen grain.

***Transmission Electron Microscopy*.** Stage 13 flowers were emasculated and pollinated on plants with mature WT pollen. One hour after pollination, pistils were immersed in fixative solution containing 2.5% glutaraldehyde and 2.5% paraformaldehyde in 0.1 M phosphate buffer (pH 7.2) and after 4 rounds of 30 min vacuum, they were incubated in fixative for 12 hours at room temperature. Pistils were then washed in phosphate buffer and further fixed in 1% osmium tetroxide in 0.1 M phosphate buffer (pH 7.2) for 1.5 hours at room temperature. After rinsing in phosphate buffer and distilled water, samples were dehydrated through an ethanol series, impregnated in increasing concentrations of SPURR resin over a period of 3 days before being polymerized at 70°C for 18 h, sectioned (65 nm sections) and imaged at 80 kV using an FEI TEM tecnaiSpirit with 4 k x 4 k eagle CCD.

***Anisotropy estimation.*** Flowers from MAP65 lines were emasculated and stigmas were observed under confocal microscope. Images were processed with ImageJ software and quantitative analyses of the average orientation and anisotropy of CMTs were performed using FibrilTool, an ImageJ plug-in[53]. Anisotropy values range from 0 to 1; 0 indicates pure isotropy, and 1 pure anisotropy.

***Membrane deformation estimation.*** Flowers from LTI6B lines were emasculated and pollinated with mature pollen from the PACT11::RFP line. 20 minutes after pollination, stigmas were observed under confocal microscope. Serial confocal images every 1 µm encompassing the entire volume of the stigma were recorded and processed with ImageJ software. Plasma membrane deformation was estimated by choosing the slide from the stack that corresponded to the focus plan of the contact site with the RFP-labelled pollen tube. On the Bright field image corresponding to the selected slide, a line was drawn connecting the two ridges of the invagination of the papilla. Two perpendicular lines, one toward the exterior (ExtD) of the papilla to the maximum point of deformation, and the other toward the interior (IntD) on the GFP image were measured, respectively.

**Statistical analysis.** Graph and statistics were obtained with R software or Excel. Statistical tests performed are specified in figure legends.

**Chemical treatment.** To avoid contact of pollen grains with liquid, we performed local applications of oryzalin (Chemical service, Supelco) at 833 µg/mL (DMSO) in lanolin pasted around the style, just under the stigmatic cells, for 4 hours at 21°C. Oryzalin-treated pistils were pollinated with mature WT pollen and 1 hour after pollination observed under SEM.

## FIGURES

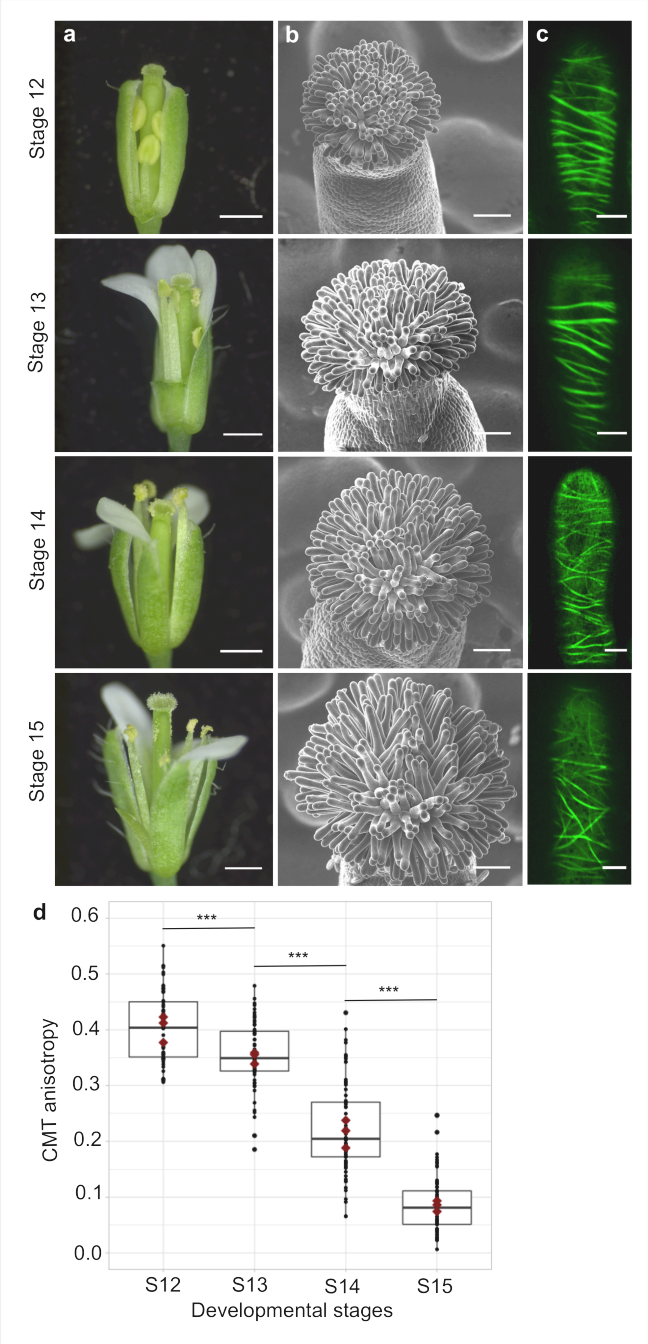


**Fig. 1| CMT organisation during papilla cell development. a**, Flower development of *A. thaliana* from developmental stages 12 to 15. Scale bar, 500 µm. **b**, Upper view of the stigma during development by SEM. Scale bar, 50 µm. **c**, Confocal images of papilla cells expressing MAP65-citrine at each stage of development. Scale bar, 5 µm. **d**, Quantitative analysis of CMT array anisotropy of papilla cells from stages 12 to 15. The red dots correspond to the mean values of the three replicates. Statistical difference were calculated using a Shapiro-Wilk test to evaluate the normality and then a Wilcoxon test, ***P < 0.01. N > 4 stigmas, n > 60 papilla cells for each stage.

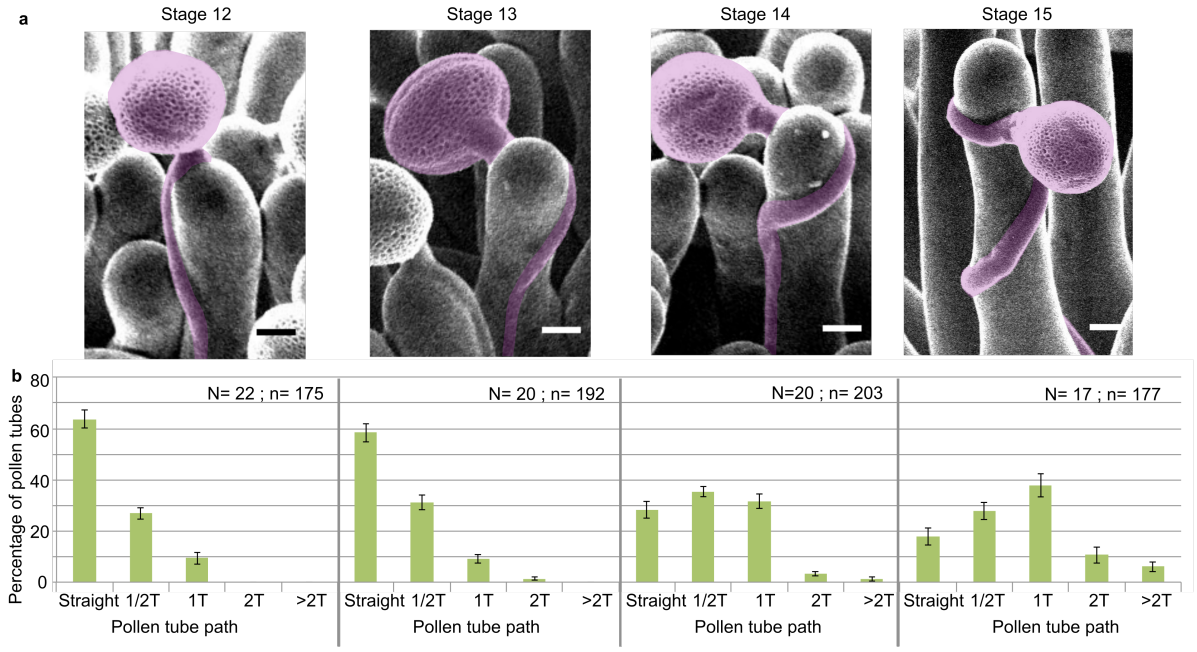


**Fig. 2| Pollen tube growth behaviour on papillae during development. a**, SEM images of Col-0 papillae pollinated with Col-0 pollen, one hour post pollination, from stages 12 to 15; pollen and tubes were artificially colorised. Scale bar, 5 µm. **b**, Quantification of the number of turns (T) made by the pollen tube on papillae from stages 12 to 15. Data are expressed as mean +/- s.e.m. A Chi-Square test for independence (at 6 degree of freedom) was used to compare all stages and demonstrated that the number of turns was significantly different between stages (***P < 0.01).

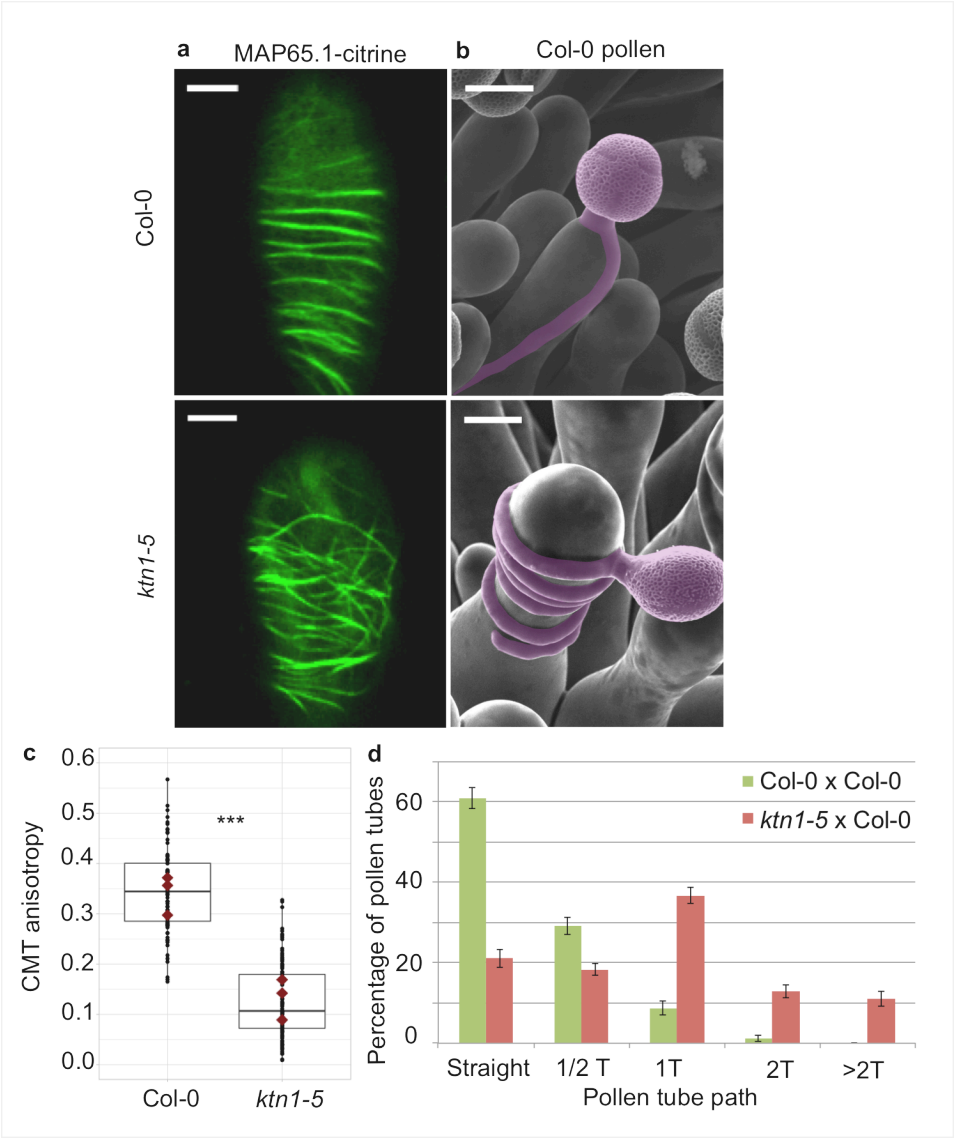


410

411 **Fig. 3| Effect of CMT organization on pollen tube path. a**, Confocal images of papilla cells
412 expressing MAP65.1-citrine in Col-0, *ktn1-5* at stage 13. Scale bars, 5 µm. **b**, SEM images of
413 Col-0 and *ktn1-5* papillae pollinated with Col-0 pollen grains; pollen and tubes were artificially
414 colorized. Scale bar, 10 µm. **c**, CMT anisotropy of Col-0 and *ktn1-5* papilla cells at stage 13.
415 N(Col-0) = 10 stigmas, n(Col-0) = 106 papillae, N(*ktn1-5*) = 11stigmas, n(*ktn1-5*) = 114
416 papillae. Statistical differences were calculated using a Shapiro-Wilk test to evaluate the
417 normality and then a Wilcoxon test with ***P < 0.01. **d**, Quantification of the number of turns
418 (T) made by Col-0 pollen tubes on *ktn1-5* and Col-0 papillae. Data are expressed as mean
419 +/- s.e.m. Statistical difference was found between pollen tube path within *ktn1-5* and Col-0
420 papillae and was calculated using an adjusted Chi-Square test for homogeneity (2 degrees of
421 freedom), ***P < 0.01. N(Col-0) = 27 stigmas, n(Col-0) = 251 papillae, N(*ktn1-5*) = 23
422 stigmas, n(*ktn1-5*) = 327 papillae.

423

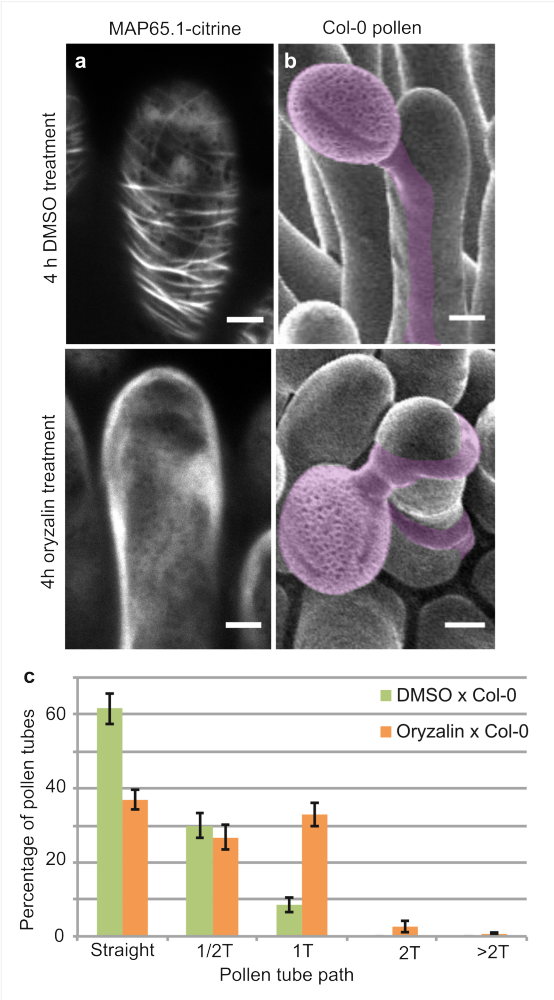


**Fig. 4| Local oryzalin application on Col-0 stigmas promotes MT destabilization and induces Col-0 pollen tube coils. a**, Col-0 papilla cells expressing MAP65.1-citrine after 4 hours of DMSO (top) or oryzalin (bottom) local treatment. **b**, SEM images of DMSO- (top) or oryzalin-treated (bottom) Col-0 stigmas pollinated with Col-0 pollen grains; pollen and tubes were artificially colorized. (a, b) Scale bars, 5 µm. **c**, Quantification of the number of turns( T) made by Col-0 pollen tubes on drug-treated and control papillae. Data are expressed as mean +/- s.e.m. Statistical difference was found between pollen tube path within DMSO (control) and oryzalin-treated papillae and was calculated using an adjusted Chi-Square test for homogeneity (2 degrees of freedom), ***P < 0.01. N(DMSO) = 12 stigmas, n(DMSO) = 117 papillae, N(oryzalin) = 16 stigmas, n(oryzalin) = 149 papillae.

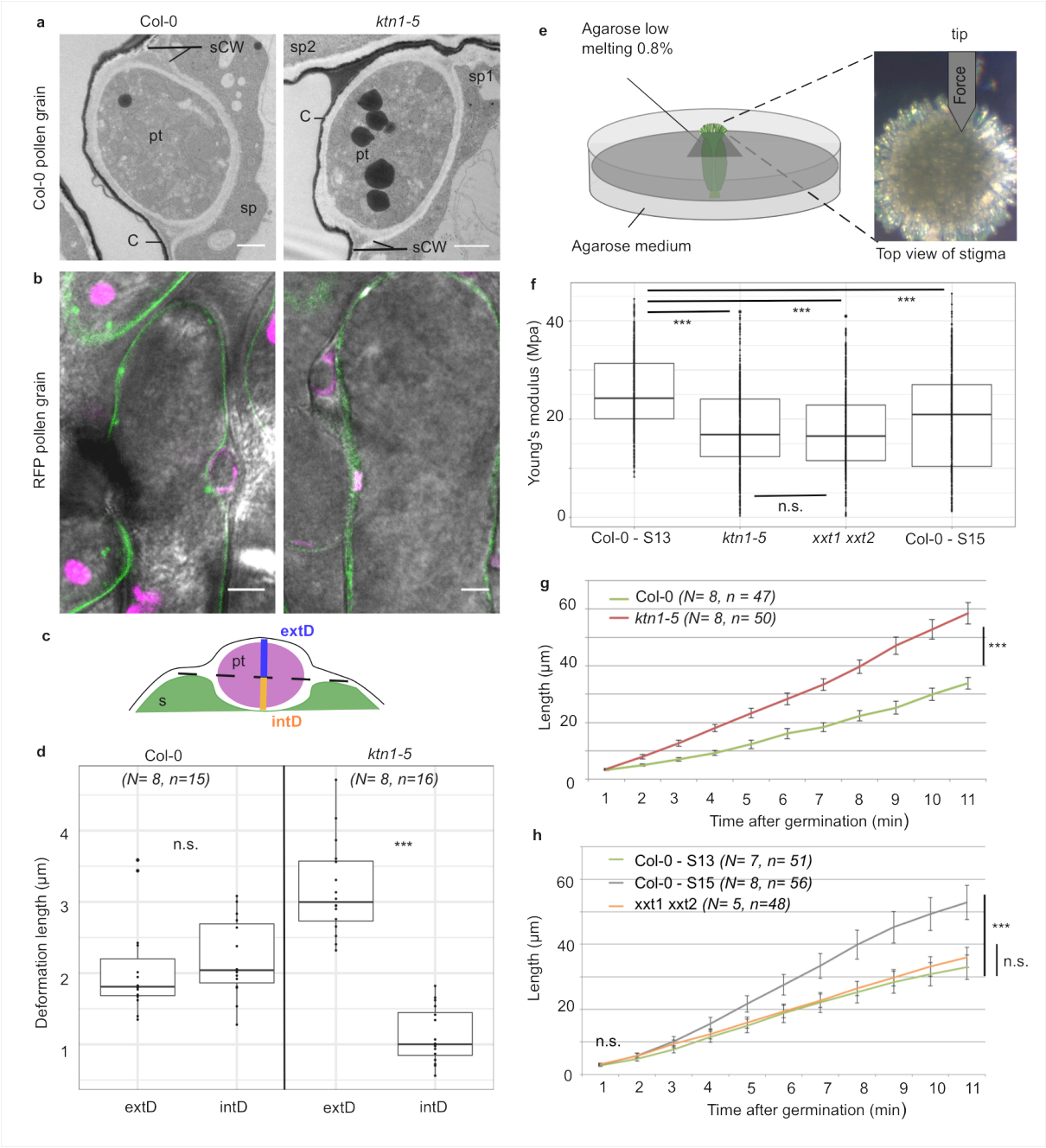


**Fig. 5| Mechanical properties of papilla cells. a**, Location of a Col-0 pollen tube in the cell-wall of Col-0 and *ktn1-5* papillae by TEM. pt = pollen tube, C = stigma cuticle, sCW = stigma cell wall, sp = stigma papilla. Scale bar, 1 µm. **b**, Confocal images of Col-0 and *ktn1-5* papillae expressing the plasma membrane marker LTI6B-GFP pollinated with an RFP-expressing pollen. Scale bar, 5 µm. **c**, Diagram showing the procedure used for evaluating the external (extD) and internal (intD) deformations made by Col-0 pollen tubes. **d**, External and internal deformations caused by Col-0 pollen tube growth in Col-0 and *ktn1-5* papillae. **e**, Drawing of the AFM experimental setup. Dissected pistils were inserted in agarose medium and fixed with low melting agarose for measurements. **f**, Young's modulus values of the papilla cell wall for Col-0 at stage 13 (N = 4 stigmas, n = 8 papillae), *ktn1-5* (N = 5 stigmas, n

= 9 papillae), *xxt1 xxt2* (N = 4 stigmas, n = 11 papillae) and Col-0 at stage15 (N = 4 stigmas, n = 10 papillae. **g**, Mean of travel distances made by Col-0 pollen tubes in Col-0 and *ktn1-5* papillae. **h**, Mean of travel distances made by Col-0 pollen tubes in papillae of Col-0 at stage 13, Col-0 at stage 15 , *xxt1 xxt2* at stage 13.

**d-e and g-h,** Statistical differences were calculated using a Shapiro-Wilk test to evaluate the normality and then a T-test. *** P < 0.01, n.s. = non significant. For h, we found a significant difference (***P < 0.01) between Col-0 at stage 13 and 15, but non significant (n.s.) between Col-0 at stage 13 and *xxt1 xxt2* at stage 13.

## SUPPLEMENTAL FIGURES

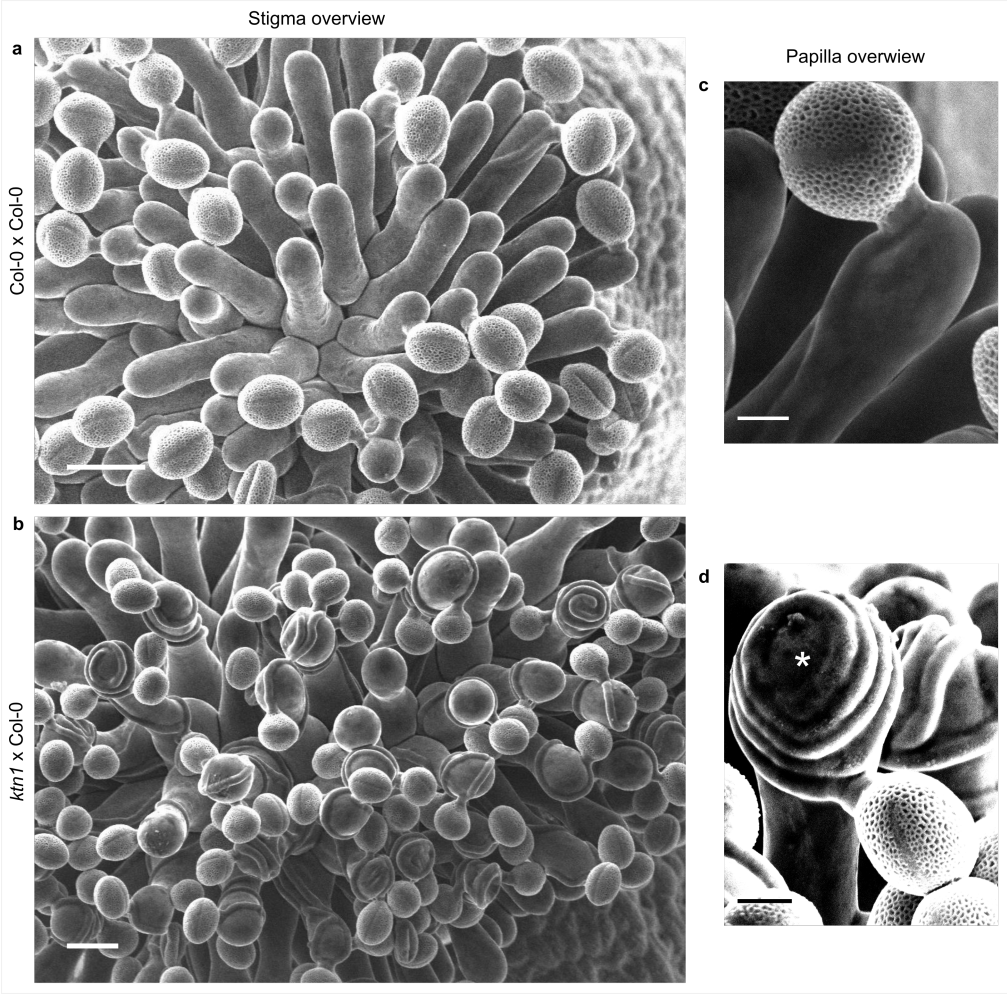


**SupFig. 1| Col-0 pollen tube behaviour on Col-0 and *ktn1-5* papillae at stage 13. a-b**, Top views of Col-0 (**a**) and *ktn1-5* (**b**) stigmas pollinated with Col-0 pollen grains. Scale bars, 20 µm. **c-d**, Magnification of pollinated papilla cells. **c**, Col-0 pollen tube grows mainly straight to the direction of the ovules on Col-0 papillae whereas **d**, it coils around and can even grow upward on *ktn1-5* papilla cells (*). Scale bars, 5 µm.

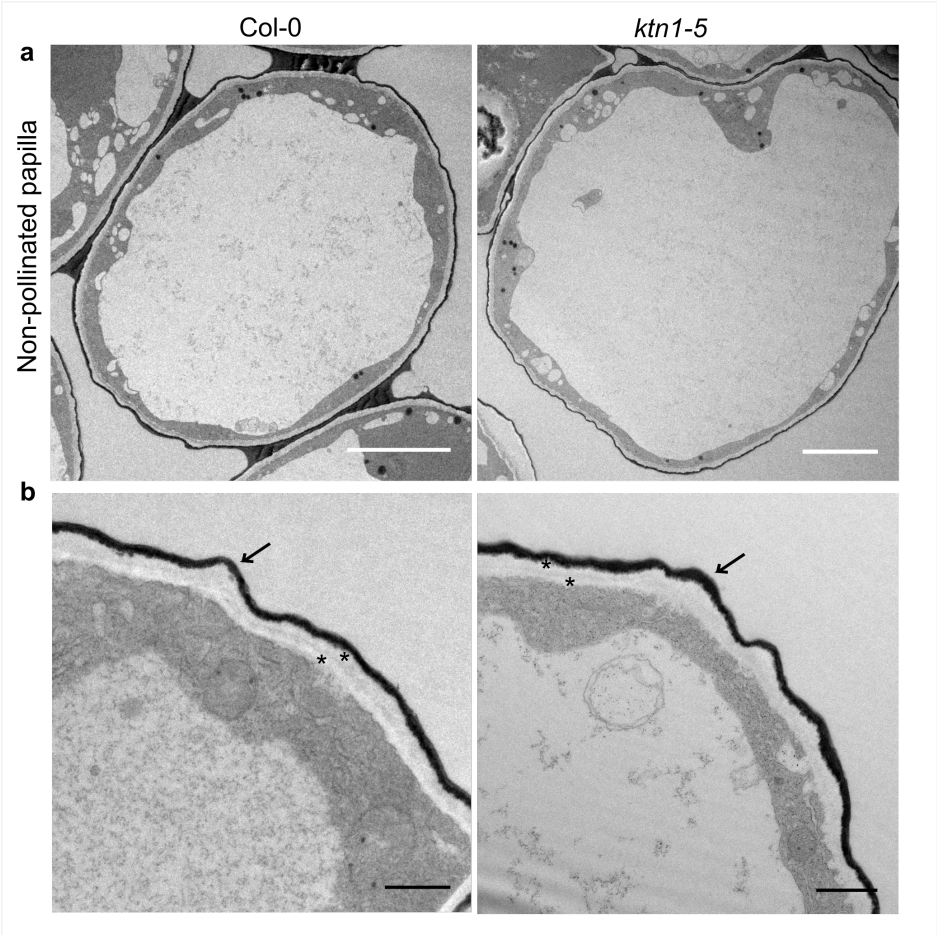


**Supfig. 2| Ultrastructure of Col-0 and *ktn1-5* papilla cells. a**, TEM images of non-pollinated Col-0 and *ktn1-5* papillae. Scale bar, 5 µm. **b**, Both Col-0 and *ktn1-5* papillae show a similar two-layered cell wall (*) delimited by a more electron dense thin layer (arrows) corresponding to the cuticle. Scale bar, 1 µm.

| Cell wall component | AGI/Name | Function* | Mutant | References |
|---|---|---|---|---|
| Cellulose | AT5G49720 *KOR1* | Endoglucanase 25 | *kor1* | 47,54,55 |
| Cellulose | AT5G64740 *PRC1* | Cellulose synthaseA catalytic subunit 6 | *prc1* | 12,43,56,57 |
| Cellulose | AT4G32410 *ANY1* | Cellulose synthaseA catalytic subunit 6 | *any1* | 44 |
| Hemicellulose | AT3G62720 *XXT1*<br>AT4G02500 *XXT2* | Xyloglucan 6-xylosyltransferase 1<br>Xyloglucan 6-xylosyltransferase 2 | *xxt1 xxt2* | 12,35 |
| Hemicellulose | AT1G68560 *XYL1* | Alpha-xylosidase 1 | *xyl1.4* | 58 |
| Pectin | AT1G78240 *QUA2* | Probable Pectin methyltransferase | *qua2.1* | 46,59,60 |

*From https://www.uniprot.org

**SupTable 1| Cell-wall mutant tested**

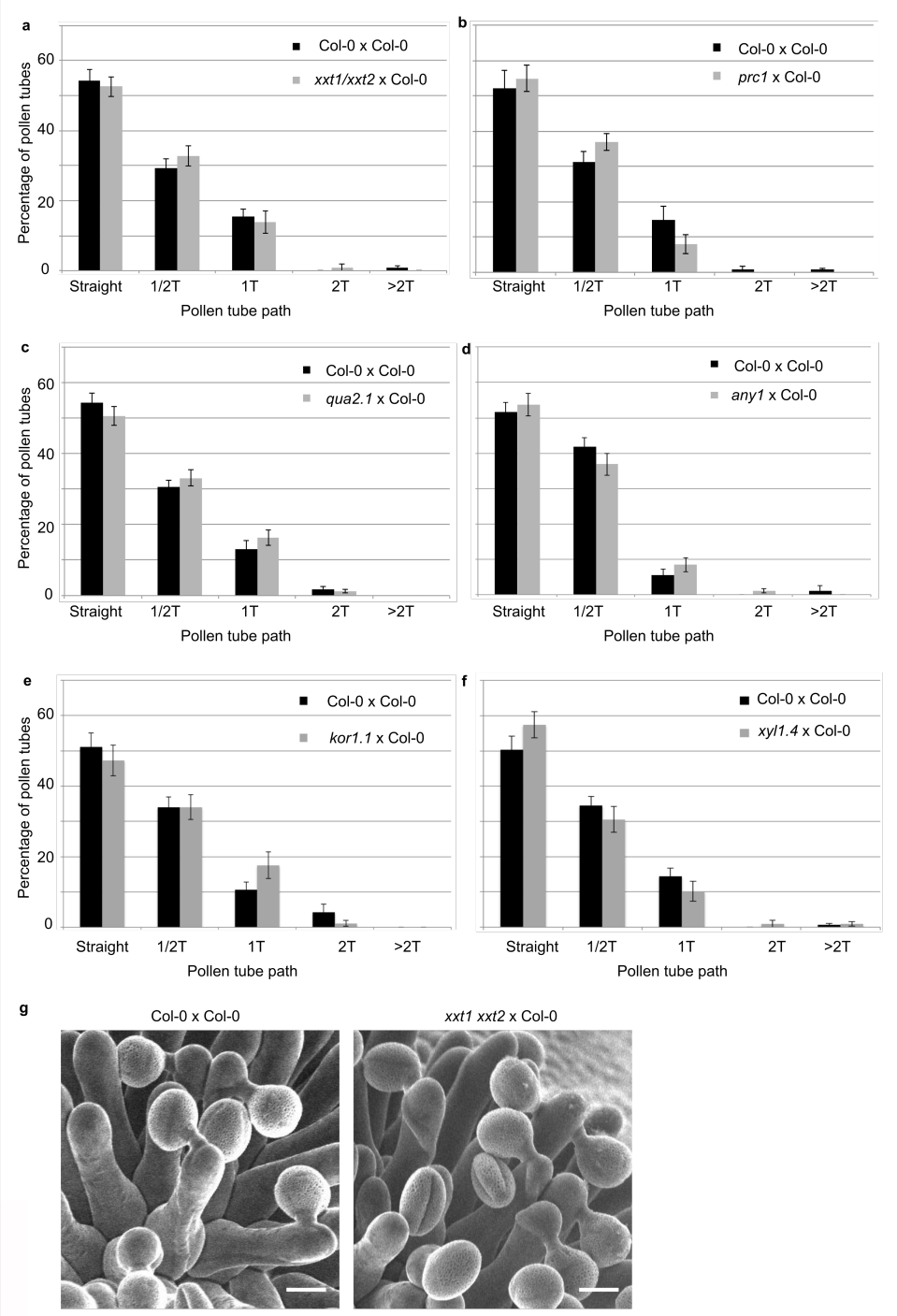


**SupFig. 3| Quantification of the number of coils made by Col-0 pollen tubes on papillae from cell-wall mutants at stage 13. a,** *xxt1 xxt2* x Col-0. N(Col-0) = 14 stigmas, n(Col-0) = 116 papillae, N(*xxt1 xxt2*) = 12 stigmas, n(*xxt1 xxt2*) = 116 papillae. **b,** *prc1* x Col-0. N(Col-0) = 14 stigmas, n(Col-0) = 115 papillae, N(*prc1*) = 12 stigmas, n(*prc1*) = 100 papillae. **c,** *qua2.1* x Col-0. N(Col-0) = 22 stigmas, n(Col-0) = 160 papillae, N(*qua2.1*) = 18 stigmas, n(*qua2.1*) = 162 papillae. **d,** *any1* x Col-0. N(Col-0) = 14 stigmas, n(Col-0) = 91

papillae, N(*any1*) = 14 stigmas, n(*any1*) = 95 papillae. **e,** *kor1.1* x Col-0. N(Col-0) = 14 stigmas, n(Col-0) = 141 papillae, N(*kor1.1*) = 11 stigmas, n(*kor1.1*) = 91 papillae. **f,** *xyl1.4* x Col-0. N(Col-0) = 18 stigmas, n(Col-0) = 136 papillae, N(*xyl1.41*) = 16 stigmas, n(*xyl1.4*) = 108 papillae. Data are expressed as mean +/- s.e.m. No statistical difference was found between pollen tube path within the cell wall mutants and Col-0 papillae based on an adjusted Chi-Square test for homogeneity (2 degrees of freedom). **g,** SEM images of Col-0 and *xxt1 xxt2* stigmas pollinated with Col-0 pollen grains. Scale bar, 10 µm.

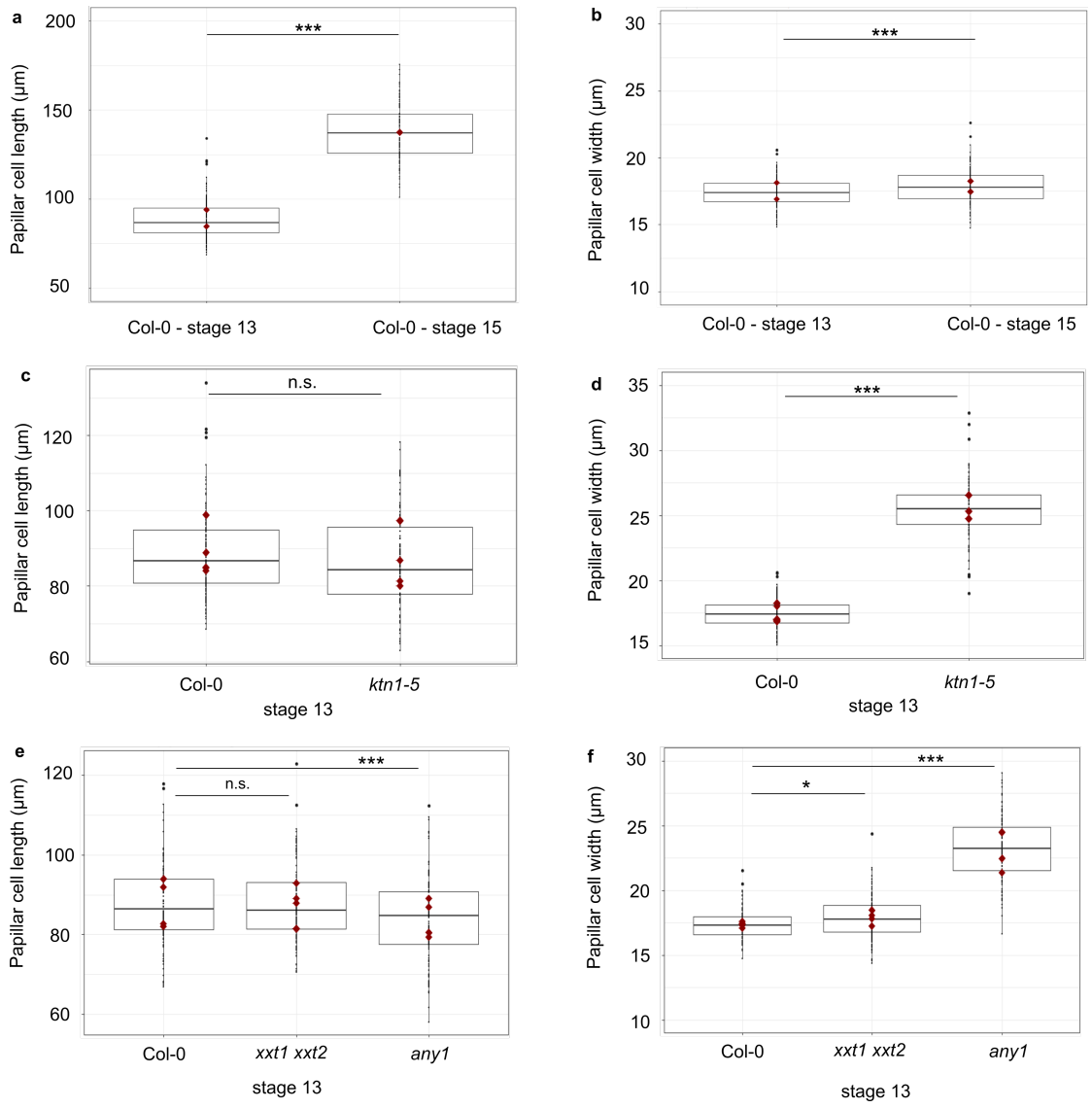


**SupFig. 4| Size of the papilla cells of Col-0 and cell wall mutants. a,** Papilla cell length of Col-0 at stage 13 and stage 15. **b,** Papilla cell width of Col-0 at stage 13 and stage 15. **c,** Papilla cell length of Col-0 and *ktn1-5* at stage 13. **d,** Papilla cell width of Col-0 and *ktn1-5* at stage 13. **e,** Papilla cell length of Col-0, *xxt1 xxt2* and *any1* at stage 13. **f,** Papilla cell width of Col-0, *xxt1 xxt2* and *any1* at stage 13. Statistical differences were calculated using a T-test. *

504 P < 0.05, *** P < 0.01, n.s. = non significant. N=4 stigmas and n=120 papillae for each
505 genotypes.

506 **Acknowledgements**

507 We thank O. Hamant for critical reading of the manuscript and fruitful discussion, A.
508 Boudaoud, S. Bovio and V. Battu for advice on AFM experiments, and the Sice and
509 MechanoDevo team members for discussion, P. Bolland, A. Lacroix and J. Berger for plant
510 care and the PLATIM imaging facility of the SFR Biosciences Gerland-Lyon Sud. We thank
511 the Bordeaux Imaging Centre especially L. Brocard and B. Batailler for TEM microscopy. We
512 also thank the BioMeca® society and Pascale Milani for the AFM measurements. L.R. was
513 funded by a fellowship from the French Ministry of Higher Education and Research. The work
514 was supported by Grant ANR-14-CE11-0021.

515 **Author contributions**

516 L.R. performed all the experiments and the image analysis, except TEM and AFM, which
517 were subcontracted. F.R. and C.K. contributed to cell imaging setup. L.R., T.G., and I.F.L.,
518 designed the study and analysed the data. L.R. and T.G. wrote the manuscript.

519 **Competing interests**

520 The authors declare no competing interests.

521

522 **References**

523 1. Lennon, K. A. & Lord, E. M. In vivo pollen tube cell of Arabidopsis thaliana I. Tube cell
524 cytoplasm and wall. *Protoplasma* **214,** 45–56 (2000).

525 2. Crawford, B. C. W. & Yanofsky, M. F. The Formation and Function of the Female
526 Reproductive Tract in Flowering Plants. *Current Biology* **18,** R972–R978 (2008).

527 3. Higashiyama, T. & Hamamura, Y. Gametophytic pollen tube guidance. *Sex Plant*
528 *Reprod* **21,** 17–26 (2008).

529 4. Discher, D. E., Janmey, P. & Wang, Y. Tissue Cells Feel and Respond to the
530 Stiffness of Their Substrate. *Science* **310,** 1139–1143 (2005).

531 5. Ermis, M., Antmen, E. & Hasirci, V. Micro and Nanofabrication methods to control
532 cell-substrate interactions and cell behavior: A review from the tissue engineering
533 perspective. *Bioactive Materials* **3,** 355–369 (2018).

534 6. Fu, J. *et al.* Mechanical regulation of cell function with geometrically modulated
535 elastomeric substrates. *Nat Methods* **7,** 733–736 (2010).

536 7. Kesten, C., Menna, A. & Sánchez-Rodríguez, C. Regulation of cellulose synthesis in
537 response to stress. *Current Opinion in Plant Biology* **40,** 106–113 (2017).

538 8. Sanati Nezhad, A. & Geitmann, A. The cellular mechanics of an invasive lifestyle.

539 *Journal of Experimental Botany* **64,** 4709–4728 (2013).

540 9. Paredez, A. R., Somerville, C. R. & Ehrhardt, D. W. Visualization of Cellulose
541 Synthase Demonstrates Functional Association with Microtubules. *Science* **312,** 1491–1495
542 (2006).

543 10. Sampathkumar, A. *et al.* Subcellular and supracellular mechanical stress prescribes
544 cytoskeleton behavior in Arabidopsis cotyledon pavement cells. *eLife Sciences* **3,** e01967
545 (2014).

546 11. Xiao, C. & Anderson, C. T. Interconnections between cell wall polymers, wall
547 mechanics, and cortical microtubules: Teasing out causes and consequences. *Plant Signal*
548 *Behav* **11,** (2016).

549 12. Xiao, C., Zhang, T., Zheng, Y., Cosgrove, D. J. & Anderson, C. T. Xyloglucan
550 Deficiency Disrupts Microtubule Stability and Cellulose Biosynthesis in Arabidopsis, Altering
551 Cell Growth and Morphogenesis1[OPEN]. *Plant Physiol* **170,** 234–249 (2016).

552 13. Louveaux, M., Rochette, S., Beauzamy, L., Boudaoud, A. & Hamant, O. The impact
553 of mechanical compression on cortical microtubules in Arabidopsis: a quantitative pipeline.
554 *Plant J* **88,** 328–342 (2016).

555 14. Uyttewaal, M. *et al.* Mechanical stress acts via katanin to amplify differences in
556 growth rate between adjacent cells in Arabidopsis. *Cell* **149,** 439–451 (2012).

557 15. Smyth, D. R., Bowman, J. L. & Meyerowitz, E. M. Early flower development in
558 Arabidopsis. *The Plant Cell* **2,** 755–767 (1990).

559 16. Fobis-Loisy, I., Chambrier, P. & Gaude, T. Genetic transformation of Arabidopsis
560 lyrata: specific expression of the green fluorescent protein (GFP) in pistil tissues. *Plant Cell*
561 *Rep.* **26,** 745–753 (2007).

562 17. Bichet, A., Desnos, T., Turner, S., Grandjean, O. & Höfte, H. BOTERO1 is required
563 for normal orientation of cortical microtubules and anisotropic cell expansion in Arabidopsis.
564 *The Plant Journal* **25,** 137–148 (2001).

565 18. Burk, D. H. & Ye, Z.-H. Alteration of Oriented Deposition of Cellulose Microfibrils by
566 Mutation of a Katanin-Like Microtubule-Severing Protein. *Plant Cell* **14,** 2145–2160 (2002).

567 19. Burk, D. H., Liu, B., Zhong, R., Morrison, W. H. & Ye, Z.-H. A Katanin-like Protein
568 Regulates Normal Cell Wall Biosynthesis and Cell Elongation. *Plant Cell* **13,** 807–828 (2001).

569 20. Kandasamy, M. K., Nasrallah, J. B. & Nasrallah, M. E. Pollen-pistil interactions and
570 developmental regulation of pollen tube growth in Arabidopsis. *Development* **120,** 3405–
571 3418 (1994).

572 21. Rotman, N. *et al.* A Novel Class of MYB Factors Controls Sperm-Cell Formation in
573 Plants. *Current Biology* **15,** 244–248 (2005).

574 22. Baskin, T. I. Anisotropic Expansion of the Plant Cell Wall. *Annual Review of Cell and*
575 *Developmental Biology* **21,** 203–222 (2005).

576 23. Mizuta, Y. & Higashiyama, T. Chemical signaling for pollen tube guidance at a glance.
577 *Journal of Cell Science* **131,** jcs208447 (2018).

578 24. Palanivelu, R. & Tsukamoto, T. Pathfinding in angiosperm reproduction: pollen tube
579 guidance by pistils ensures successful double fertilization. *Wiley Interdisciplinary Reviews:*
580 *Developmental Biology* **1,** 96–113 (2012).

581 25. Cameron, C. & Geitmann, A. Cell mechanics of pollen tube growth. *Current Opinion*
582 *in Genetics & Development* **51,** 11–17 (2018).

583 26. Dresselhaus, T. & Franklin-Tong, N. Male–Female Crosstalk during Pollen
584 Germination, Tube Growth and Guidance, and Double Fertilization. *Molecular Plant* **6,** 1018–
585 1036 (2013).

586 27. Higashiyama, T. & Yang, W. Gametophytic Pollen Tube Guidance: Attractant
587 Peptides, Gametic Controls, and Receptors1[OPEN]. *Plant Physiol* **173,** 112–121 (2017).

588 28. Fu, Y. The cytoskeleton in the pollen tube. *Current Opinion in Plant Biology* **28,** 111–
589 119 (2015).

590 29. Gossot, O. & Geitmann, A. Pollen tube growth: coping with mechanical obstacles
591 involves the cytoskeleton. *Planta* **226,** 405–416 (2007).

592 30. Iwano, M. *et al.* Actin Dynamics in Papilla Cells of Brassica rapa during Self- and
593 Cross-Pollination. *Plant Physiol* **144,** 72–81 (2007).

594 31. Samuel, M. A. *et al.* Proteomic Analysis of Brassica Stigmatic Proteins Following the
595 Self-incompatibility Reaction Reveals a Role for Microtubule Dynamics During Pollen
596 Responses. *Mol Cell Proteomics* **10,** (2011).

597 32. Landrein, B. & Hamant, O. How mechanical stress controls microtubule behavior and
598 morphogenesis in plants: history, experiments and revisited theories. *The Plant Journal* **75,**
599 324–338 (2013).

600 33. Ryden, P. *et al.* Tensile Properties of Arabidopsis Cell Walls Depend on Both a
601 Xyloglucan Cross-Linked Microfibrillar Network and Rhamnogalacturonan II-Borate
602 Complexes. *Plant Physiol* **132,** 1033–1040 (2003).

603 34. Sassi, M. *et al.* An Auxin-Mediated Shift toward Growth Isotropy Promotes Organ
604 Formation at the Shoot Meristem in Arabidopsis. *Current Biology* **24,** 2335–2342 (2014).

605 35. Cavalier, D. M. *et al.* Disrupting Two Arabidopsis thaliana Xylosyltransferase Genes
606 Results in Plants Deficient in Xyloglucan, a Major Primary Cell Wall Component. *The Plant*
607 *Cell* **20,** 1519–1537 (2008).

608 36. Park, Y. B. & Cosgrove, D. J. Changes in Cell Wall Biomechanical Properties in the
609 Xyloglucan-Deficient xxt1/xxt2 Mutant of Arabidopsis1. *Plant Physiol* **158,** 465–475 (2012).

610 37. Takáč, T., Šamajová, O., Pechan, T., Luptovčiak, I. & Šamaj, J. Feedback
611 Microtubule Control and Microtubule-Actin Cross-talk in *Arabidopsis* Revealed by Integrative
612 Proteomic and Cell Biology Analysis of *KATANIN 1* Mutants. *Molecular & Cellular Proteomics*
613 **16,** 1591–1609 (2017).

614 38. Crowell, E. F. *et al.* Differential Regulation of Cellulose Orientation at the Inner and
615 Outer Face of Epidermal Cells in the Arabidopsis Hypocotyl. *The Plant Cell* **23,** 2592–2605
616 (2011).

617 39. Zhang, T., Mahgsoudy-Louyeh, S., Tittmann, B. & Cosgrove, D. J. Visualization of the
618 nanoscale pattern of recently-deposited cellulose microfibrils and matrix materials in never-
619 dried primary walls of the onion epidermis. *Cellulose* **21,** 853–862 (2014).

620 40. Nezhad, A. S., Naghavi, M., Packirisamy, M., Bhat, R. & Geitmann, A. Quantification
621 of cellular penetrative forces using lab-on-a-chip technology and finite element modeling.
622 *PNAS* **110,** 8093–8098 (2013).

623 41. Koser, D. E. *et al.* Mechanosensing is critical for axon growth in the developing brain.
624 *Nat Neurosci* **19,** 1592–1598 (2016).

625 42. Dong, J. Plantacyanin Plays a Role in Reproduction in Arabidopsis. *PLANT*
626 *PHYSIOLOGY* **138,** 778–789 (2005).

627 43. Fagard, M. *et al.* PROCUSTE1 Encodes a Cellulose Synthase Required for Normal
628 Cell Elongation Specifically in Roots and Dark-Grown Hypocotyls of Arabidopsis. *Plant Cell*
629 **12,** 2409–2423 (2000).

630 44. Fujita, M. *et al.* The anisotropy1 D604N mutation in the Arabidopsis cellulose
631 synthase1 catalytic domain reduces cell wall crystallinity and the velocity of cellulose
632 synthase complexes. *Plant Physiol.* **162,** 74–85 (2013).

633 45. Lin, D. *et al.* Rho GTPase Signaling Activates Microtubule Severing to Promote
634 Microtubule Ordering in Arabidopsis. *Current Biology* **23,** 290–297 (2013).

635 46. Mouille, G. *et al.* Homogalacturonan synthesis in Arabidopsis thaliana requires a
636 Golgi-localized protein with a putative methyltransferase domain. *The Plant Journal* **50,** 605–
637 614 (2007).

638 47. Nicol, F. *et al.* A plasma membrane-bound putative endo-1,4-beta-D-glucanase is
639 required for normal wall assembly and cell elongation in Arabidopsis. *EMBO J* **17,** 5563–
640 5576 (1998).

641 48. Sampedro, J. *et al.* Lack of α-Xylosidase Activity in Arabidopsis Alters Xyloglucan
642 Composition and Results in Growth Defects1[W][OA]. *Plant Physiol* **154,** 1105–1115 (2010).

643 49. Shoji, T. *et al.* Plant-Specific Microtubule-Associated Protein SPIRAL2 Is Required for
644 Anisotropic Growth in Arabidopsis. *Plant Physiology* **136,** 3933–3944 (2004).

645 50. Hellens, R. P., Edwards, E. A., Leyland, N. R., Bean, S. & Mullineaux, P. M. pGreen:
646 a versatile and flexible binary Ti vector for Agrobacterium-mediated plant transformation.
647 *Plant Molecular Biology* **42,** 819–832 (2000).

648 51. Karimi, M., Inzé, D. & Depicker, A. GATEWAY™ vectors for Agrobacterium-mediated
649 plant transformation. *Trends in Plant Science* **7,** 193–195 (2002).

650 52. Logemann, E., Birkenbihl, R. P., Ülker, B. & Somssich, I. E. An improved method for
651 preparing Agrobacterium cells that simplifies the Arabidopsis transformation protocol. *Plant*

652 *Methods* **2,** 16 (2006).

653 53. Boudaoud, A. *et al.* FibrilTool, an ImageJ plug-in to quantify fibrillar structures in raw
654 microscopy images. *Nature Protocols* **9,** 457–463 (2014).

655 54. His, I. & Driouich, A. Altered pectin composition in primary cell walls of korrigan, a
656 dwarf mutant of Arabidopsis de®cient in a membrane-bound endo-1,4-b-glucanase. 11
657 (2001).

658 55. Lei, L. *et al.* The jiaoyao1 Mutant Is an Allele of korrigan1 That Abolishes
659 Endoglucanase Activity and Affects the Organization of Both Cellulose Microfibrils and
660 Microtubules in Arabidopsis[C][W]. *Plant Cell* **26,** 2601–2616 (2014).

661 56. MacKinnon, I. M. *et al.* Cell-wall structure and anisotropy in procuste, a cellulose
662 synthase mutant of Arabidopsis thaliana. *Planta* **224,** 438–448 (2006).

663 57. Panteris, E., Adamakis, I.-D. S., Daras, G. & Rigas, S. Cortical microtubule patterning
664 in roots of Arabidopsis thaliana primary cell wall mutants reveals the bidirectional interplay
665 with cell expansion. *Plant Signal Behav* **9,** (2014).

666 58. Shigeyama, T. *et al.* α-Xylosidase plays essential roles in xyloglucan remodelling,
667 maintenance of cell wall integrity, and seed germination in Arabidopsis thaliana. *J Exp Bot*
668 **67,** 5615–5629 (2016).

669 59. Abasolo, W. *et al.* Pectin May Hinder the Unfolding of Xyloglucan Chains during Cell
670 Deformation: Implications of the Mechanical Performance of Arabidopsis Hypocotyls with
671 Pectin Alterations. *Molecular Plant* **2,** 990–999 (2009).

672 60. Verger, S., Long, Y., Boudaoud, A. & Hamant, O. A tension-adhesion feedback loop
673 in plant epidermis. *eLife* (2018). doi:10.7554/eLife.34460

674